Available online at www.sciencedirect.com
ScienceDirect
Journal of Catalysis 251 (2007) 48–58
JOURNAL OF CATALYSIS
www.elsevier.com/locate/jcat

Insight into the nature of active redox sites in Ru-containing hydroxyapatite by DRIFT spectroscopy

Z. Opre, D. Ferri, F. Krumeich, T. Mallat, A. Baiker *

Institute for Chemical and Bioengineering, Department of Chemistry and Applied Bioscience, ETH Zurich, Hönggerberg, HCI, CH 8093 Zurich, Switzerland

Received 23 April 2007; revised 16 July 2007; accepted 17 July 2007

Available online 23 August 2007

Abstract

The excellent selectivity and activity of ruthenium-hydroxyapatite {RuHAp, HAp = $Ca_{10}(PO_4)_6(OH)_2$} in the aerobic oxidation of alcohols has been attributed to isolated, monomeric Ru^{3+} species as the active sites. Here we reinvestigated these catalysts by a DRIFT study of CO adsorption and by electron microscopy (STEM) combined with EDX analysis. The study revealed the presence of two major species: isolated Ru^{3+} ions and hydrated Ru^{3+}-oxide particles. The latter structure has high redox activity; it is easily oxidized with oxygen to RuO_2 and reduced by hydrogen or CO at ambient conditions. The amount of this phase in the catalysts correlates well with the alcohol oxidation activity in the liquid phase at close to ambient conditions. In contrast, the redox activity of isolated Ru^{3+} ions is significantly lower (or they might be completely inactive). These species may correspond to adsorbed Ru^{3+} ions, ion-exchanged Ru^{3+} at the outer surface of HAp, or Ru^{3+} ions in Ru-phosphate formed by a dissolution–redeposition process from HAp. Our final conclusion is that in RuHAp, the real active sites are small hydrated Ru^{3+}-oxide nanoparticles (1–2 nm) located on the surface of HAp. Application of a low $RuCl_3$ concentration and a short contact time between HAp and the aqueous $RuCl_3$ solution during catalyst preparation help maximize the fraction of the Ru^{3+}-oxide phase and thus the catalytic activity.

Keywords: Hydroxyapatite; Ruthenium; Redox sites; Hydrated ruthenium oxide nanoparticles; DRIFT spectroscopy; CO adsorption; Aerobic oxidation of alcohols

1. Introduction

Hydroxyapatite-based materials have generated great interest in the past years as solid, recyclable catalysts of a wide range of organic reactions [1–5]. The broad applicability is achieved by a partial replacement of Ca^{2+} ions in the lattice of hydroxyapatite [HAp, $Ca_{10}(PO_4)_6(OH)_2$] with 1–4 valent metal ions [6–8]. A widely used representative is ruthenium-hydroxyapatite (RuHAp), which can be prepared by immersion of HAp in an aqueous $RuCl_3$ solution (soaking) under ambient conditions [9]. RuHAp is a highly selective catalyst for the partial oxidation of alcohols [9–13], amines [14], and organosilanes [15] using molecular oxygen as the sole oxidant. The catalytic material is also effective in Diels–Alder and aldol reactions [16], as well as in the racemization of configurationally stable chiral secondary alcohols [17]. The excellent performance of RuHAp is attributed to its bifunctional character: the redox activity of the Ru sites and the basic sites in the apatite lattice. A thorough structural optimization, including fine tuning of the amount and location of Ru and maintenance of the hydrated form of RuHAp at the end of the synthesis, resulted in a 100-fold enhancement of activity in alcohol oxidation [9,12].

There is no agreement concerning the nature of active sites in Ru-containing hydroxyapatites. Kaneda's group, who first described the synthesis and catalytic application of RuHAp, assumed ion exchange between Ru^{3+} and Ca^{2+} ions [10]. They proposed, based on XANES data, that ruthenium in the "hybrid heterogeneous catalyst" exists as a monomeric phosphatoruthenium complex surrounded by one chloride atom and four oxygen atoms (provided by two PO_4 tetrahedra). In contrast, Wuyts et al. found no chlorine by XPS and ICP analysis in RuHAp and suggested the presence of mononuclear, chlorine-free Ru^{3+} species located mainly at the outer rim of the HAp crystals [17]. We confirmed by ICP-OES, XPS, and EXAFS analysis that chlorine is present in RuHAp only in trace amounts, probably as an adsorbed impurity but not as a component of the active

* Corresponding author.
E-mail address: baiker@chem.ethz.ch (A. Baiker).

0021-9517/$ – see front matter
doi:10.1016/j.jcat.2007.07.017

species [11]. The EXAFS study indicated that the first shell surrounding ruthenium on RuHAp consists of two hydroxy ligands and four oxygen atoms bound to two phosphorus atoms. Recently, Tonsuaadu et al. concluded from EXAFS measurements that the Ru^{3+} ions are surrounded by six oxygen atoms and chlorine is not present in the first two shells surrounding the Ru^{3+} ions [13]; this interpretation is in line with our results.

Although it has been proposed based on EXAFS analysis that Ru-containing hydroxyapatites [10,18] and zeolites [19] display monomeric Ru species, X-ray-based techniques are not able to distinguish between species in catalytic systems exhibiting several different types of metal and cationic centers but rather give an average structure. Thus, EXAFS indicated that the environment of Ru in the different RuHAp catalysts is similar [11]. IR spectroscopy is more sensitive to the nature of structurally different species. In general, a probe molecule is chosen in a way that the adsorbate shows a specific absorption energy, which is different from that exhibited by its neighbors when these are of different structure. However, infrared spectra may appear more complex due to surface processes, including reduction, oxidation, and particle disruption induced by adsorption of the probe molecule. This drawback can be overcome by running measurements at the temperature of liquid nitrogen, which on the other hand are conditions different from that under which the catalytic materials are used. Adsorption of carbon monoxide followed by infrared spectroscopy is a widely used tool to characterize well-dispersed metals supported on metal oxides, because the stretching vibration of CO is sensitive to the environment and the structure of the adsorption site [20]. Consequently, several features can be observed on the specimen in which the metal is present in the form of ions and easily reducible species that complicate the interpretation of the infrared spectra. Adsorption of CO on supported Ru is such an example.

In general, ion exchange by diffusion into the HAp lattice [21–24] is not the only mechanism considered for the development of M^{n+}-promoted HAp. Other favored explanations are the adsorption of metal ions (e.g., Cd^{2+} [25]) and dissolution–precipitation-type mechanisms [26–28]. In the light of literature data and our previous experiments, we doubt that a simple ion exchange between ruthenium and calcium ions in the apatite channels can describe the formation of active RuHAp. We found that after contacting HAp with the aqueous $RuCl_3$ solution, the pH increased rapidly and more than stoichiometric amount of Ca^{2+} and considerable amount of PO_4^{3+} appeared in solution [9]. XRD and thermal analysis revealed that with increasing contact time between HAp and aqueous $RuCl_3$, the crystallite size and thermal stability of the materials decreased, and the restructuring was also confirmed by XPS. We observed some restructuring and a considerable loss of oxidation activity also by heat treatment of the catalyst at or above 80 °C. This phenomenon, which is typical for hydrated ruthenium oxide [29,30], cannot easily be interpreted by the assumption of monomeric Ru species as the active sites formed by cation exchange [10,18].

Intrigued by these observations we reinvestigated the structure of RuHAp with a focus on DRIFT spectroscopy. This study confirms our former speculation that the real active sites are probably very small, hydrated ruthenium oxide nanoparticles deposited on the outer surface of HAp.

Table 1
Characterization of the RuHAp catalysts used in the present study

Catalyst	Contact time between HAp and aq. $RuCl_3$	Ru content (wt%)	BET surface area (m^2/g)
RuHAp-10 min	10 min	2.6	78
RuHAp-24 h	24 h	3.2	75
14.5 wt% RuHAp-24 h	24 h	14.5	85

2. Experimental

2.1. Catalyst preparation

Starting materials for catalyst preparation were $RuCl_3$ hydrate (36% Ru, 99.9%, ABCR), aqueous ammonia solution (ca. 25% NH_3, Merck), $(NH_4)_2HPO_4$ (98%, ABCR), and $Ca(NO_3)_2{\cdot}4H_2O$ (99%, Strem Chemicals). Stoichiometric calcium hydroxyapatite $Ca_{10}(PO_4)_6(OH)_2$ (HAp) was synthesized by a wet chemical method according to a known procedure and calcined at 500 °C for 3 h [31]. Next we introduced ruthenium by shaking HAp (1.0 g) with 75 mL of a 6.7 mM aqueous $RuCl_3$ solution at room temperature for 10 min or 24 h. The catalysts were filtered off, washed with deionized water, and dried overnight at room temperature in vacuum. The time indicated in the abbreviation of the catalyst designation (10 min or 24 h) indicates the contact time of the $RuCl_3$ solution with HAp. The designation of the catalysts, the Ru content determined by inductively coupled plasma optical emission spectroscopy (ICP-OES), and BET surface areas are summarized in Table 1.

The RuHAp-24 h catalyst was prepared also with higher Ru content. In this case, the ruthenium concentration of the aqueous $RuCl_3$ solution was 2.67×10^{-2} M. This catalyst contained 14.5 wt% Ru; the difference between the actual and the calculated Ru content (17 wt%) originates mainly from the adsorbed water, which was not removed by drying at room temperature in vacuum. The abbreviation used for this catalyst is 14.5 wt% RuHAp-24 h.

2.2. Characterization techniques

The BET surface area and pore size distribution were determined by N_2 adsorption–desorption at 77 K using a Micromeritics ASAP 2010 instrument. Before measurement, the samples were degassed in vacuum at 60 °C. The Ru concentration of the catalysts (after dissolution in HNO_3) was determined by ICP-OES.

The hydrogen consumption during reduction of the catalysts was measured using the double-isotherm method [32] (Micromeritics ASAP 2010 Multigas system). The samples were degassed for 2 h at 40 °C, then adsorption isotherms were measured at 40 °C. After the first isotherm was recorded, the cell was outgassed for 10 min at 40 °C, and a second isotherm was

measured. The amount of hydrogen (H) consumed for the (partial) reduction of Ru^{n+} in the catalyst was determined by taking the difference between the isotherms.

For scanning transmission electron microscopy (STEM), the samples were suspended in ethanol, and some droplets deposited on a holey carbon foil supported on a copper grid. The investigation was performed on a field emission transmission electron microscope Tecnai 30F (FEI; SuperTwin lens with $C_s = 1.2$ mm), operated at 300 kV. STEM images were recorded with a high-angle annular dark field (HAADF) detector, using almost exclusively incoherently scattered electrons (Rutherford scattering) for getting images with atomic number (Z) contrast [33]. An energy-dispersive X-ray (EDX) spectrometer attached to the Tecnai F30 allowed elemental analyses at areas with diameters of 30–40 nm selected in the HAADF-STEM images [34].

Diffuse reflectance infrared (DRIFT) spectra were collected with an Equinox 55 spectrometer (Bruker Optics) at a resolution of 4 cm^{-1}. The instrument was equipped with a HVC-DRP2 reaction chamber (Harrick) and a liquid nitrogen-cooled MCT detector. The gas flow rates were always 10 mL/min. The CO adsorption spectra were taken at 25 °C in a 10% CO/Ar flow on pure catalyst powders and the spectra after adsorption of CO followed by desorption were taken at different temperatures in an Ar flow. The results given herein are difference spectra where the spectrum of the sample before admission of CO to the cell served as the reference. Spectra obtained at different temperatures after CO adsorption were acquired with the same reference, which procedure can cause negative features in the region of the overtone and combination bands of the phosphate groups (2200–1900 cm^{-1}). To obtain information from the skeletal vibrations of the materials, the single channel spectrum of the different samples was ratioed against KBr. In situ heat treatments were carried out by increasing the sample temperature at 10 °C/min to the desired temperature in an Ar flow, and held at that temperature for 1 h. Then the temperature was decreased to 25 °C in Ar. The reduction treatments were carried out at 300 °C in a 10% H_2/Ar flow for 1 h. Then the catalyst was cooled to 100 °C in a 10% H_2/Ar flow, further to 25 °C in Ar, and it was kept at 25 °C in Ar flow for 30 min. The oxidation treatments were carried out at 90 °C or room temperature in an O_2 flow for 1 h. Then the catalyst was cooled to 25 °C in Ar. Band deconvolution was performed using the fit utility of the software OPUS and mixed Laurentzian–Gaussian functions.

3. Results and discussion

3.1. DRIFT spectroscopy

The infrared spectrum of hydroxyapatite (HAp) (Fig. 1a) exhibits characteristic features related to the skeletal vibrations of the lattice phosphate groups (below 1300 cm^{-1}) and of the surface (above 3580 cm^{-1}) and lattice (3571 cm^{-1}) hydroxyl groups [35]. Addition of Ru to HAp (Fig. 1b) does not result in the appearance of any additional spectral feature, unless the sample is heated above 100 °C, in which case a new signal appears at ca. 1880 cm^{-1}, as reported earlier [9]. The surface of

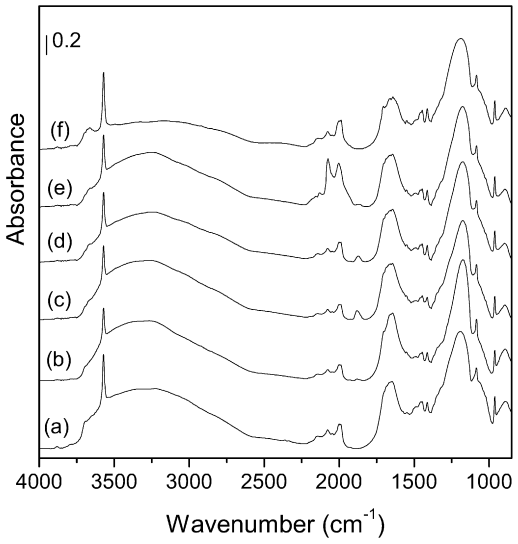

Fig. 1. DRIFT spectra of HAp (a), RuHAp-10 min (b), RuHAp-10 min pretreated in O_2 at RT (c), RuHAp-10 min pretreated in Ar at 90 °C (d), RuHAp-10 min pretreated in Ar at 90 °C and after CO adsorption (e), and RuHAp-10 min pretreated in H_2 at 300 °C (f).

the as-prepared material is covered by water, as indicated in Fig. 1 by the broad band extending over the 3700–2500 cm^{-1} range and by the band at ca. 1640 cm^{-1}. Signals between 1600 and 1300 cm^{-1} are characteristic of carbonate species produced after exposure of the sample to air.

The time-dependent adsorption of CO on the as-prepared RuHAp-10 min at room temperature is shown in Fig. 2. In the early stages of adsorption, three bands are discernible at ca. 2066, 2051, and 2012 cm^{-1}. After 1 h adsorption time, five bands appear in the IR spectra at 2135, 2075, 2049, and 2006 cm^{-1}, and a broad band below 2000 cm^{-1}. All five bands resist desorption at room temperature (30 min in an Ar flow; Fig. 2b). The band at 2135 cm^{-1} is partially covered by the signals of gaseous CO and becomes clear only when purging with Ar (Fig. 2b). Identical experiments on HAp did not result in the appearance of adsorbed CO, which typically exhibits a band at ca. 2170 cm^{-1} only at low temperature [36,37].

Band deconvolution reveals that the spectrum obtained after 1 h adsorption time is actually composed of additional bands besides those that are clearly visible (an illustration of deconvolution is given in Fig. 2d). Two bands at 1971 and 1933 cm^{-1} have to be taken into account on the low-energy side of the complex envelope, and two other bands at 2081 and 2069 cm^{-1} to fit the band at 2075 cm^{-1}. Moreover, the asymmetry of the band at 2006 cm^{-1} suggests that it is composed of two bands close in energy, but their involvement is not required for a good deconvolution.

The negative feature at ca. 1650 cm^{-1} reveals that water molecules are displaced during CO adsorption. Water desorption likely is also the origin of other spectral changes. The high-frequency region (not shown) exhibits a broad negative feature with a maximum at approximately 3520 cm^{-1} accompanied by a broad positive band at ca. 3250 cm^{-1}. Similarly, the weak negative band at 3695 cm^{-1} and the positive signal at 3570 cm^{-1} indicate removal of water adsorbed on the P–OH

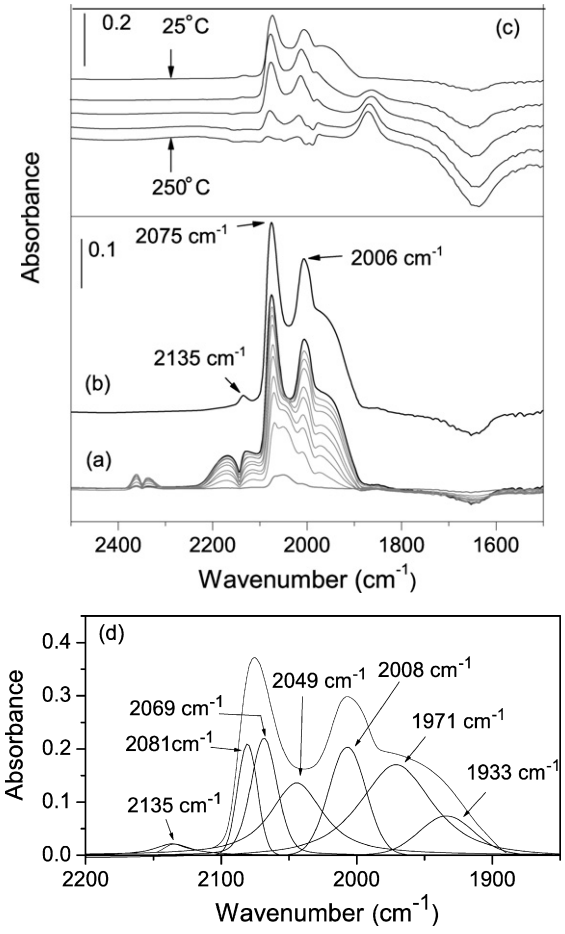

Fig. 2. (a) Time-resolved DRIFT spectra taken during CO adsorption at 25 °C on RuHAp-10 min. (b) DRIFT spectrum recorded after 30 min under Ar flow subsequent to CO adsorption. (c) DRIFT spectra of RuHAp-10 min after adsorption of CO followed by desorption in Ar at 25, 100, 150, 200, and 250 °C. (d) Deconvolution of the DRIFT spectrum shown in (b).

and OH groups of the apatite network, respectively. Formation of additional carbonate species was not observed during CO adsorption. Assignment of the observed spectral changes above 3000 cm^{-1} to specific changes produced by adsorption of CO is not straightforward because of the presence of large amount of adsorbed water. (Removal of water by heat treatment at elevated temperature may solve this problem [38,39], but this treatment induces significant restructuring and a loss of catalytic activity of RuHAp [9].) Therefore, the following discussion is limited to the features appearing in the carbonyl region of the spectra.

Adsorption of CO caused the reduction of Ru^{n+} ions in RuHAp-10 min and the amount of the evolved CO_2 co-product reached a maximum after ca. 7 min (Fig. 2a). Evolution of CO_2 can be followed by the band at 2049 cm^{-1} that appeared rapidly and was then slightly attenuated compared to the other bands. Reduction of Ru^{n+} by CO adsorption renders identification of Ru-species in the original sample more difficult. According to the literature, reviewed by Hadjiivanov and Vayssilov [20], all bands observed in Fig. 2 are most likely characteristic for ionic Ru carbonyl species [$Ru^{n+}(CO)_x$ with $x, n = 1$–3]. Table 2 summarizes the assignment of the major signals observed on RuHAp and on several other Ru-containing materials that are relevant for the present discussion. Ru carbonyl bands at around the same frequency as that shown in Fig. 2 have been observed previously in the literature, although some assignments are still debated. Adsorbed CO on Ru cations is typically ordered into carbonyl species of type I (Ru^0–CO), type II [multicarbonyl, $Ru^{n+}(CO)_x$] and type III [dicarbonyl, $Ru^{n+}(CO)_2$], which are characterized by a low-frequency signal (LF, type I), a set of high-frequency signals (HF_1 and HF_2, type II) and by a set of HF_2 and LF signals (type III), respectively. The characteristic absorption bands corresponding to each feature appear commonly at 2060–2000 cm^{-1} (LF), 2160–2120 cm^{-1} (HF_1), at 2110–2060 cm^{-1} (HF_2) [40]. For example, the band at 2135 cm^{-1} (HF_1) that is typically associated with a component at 2055 cm^{-1} (HF_2) was assigned to the asymmetric and symmetric stretching of a $Ru^{3+}(CO)_2$ species [41], whereas the bands at 2070 (HF_2) and 2004 cm^{-1} (LF) were assigned to those of a $Ru^{2+}(CO)_2$ species on oxidized Ru/ZrO_2. The bands at 2142 and 2084 cm^{-1} were assigned to $Ru^{n+}(CO)_3$ multicarbonyls on oxidized Ru/TiO_2, a part of the band at 2084 cm^{-1} to Ru^{n+}–CO monocarbonyl, and the band at 2036 cm^{-1} to ionic dicarbonyls [40]. Following the assignments discussed in the literature, we attribute the bands at 2135 and 2075 cm^{-1} in the RuHAp-10 min sample to $Ru^{3+}(CO)_3$ multicarbonyls. However, part of the latter band may also correspond to a $Ru^{n+}(CO)_2$ dicarbonyl, which is accompanied by the additional band at 2006 cm^{-1}. This explains why two bands are needed to fit this band in the spectrum of adsorbed CO.

The asymmetric broadening below 2000 cm^{-1} entangling two signals at 1971 and 1934 cm^{-1} (as from spectrum deconvolution) has already been observed [42]. Bands at 1995 and 1950 cm^{-1} were assigned to the monocarbonyl form of CO linearly bonded to oxidized ruthenium in different oxidation states, with the general formula $Ru^{n+}O_x(CO)$. In the case of Ru/MgO, a signal at 1975 cm^{-1} was associated with bridged species of the type O–Ru–C(O)–Ru–O [43]. In our case, the signals at 1971 and 1934 cm^{-1} probably indicate the presence of Ru^{n+} entities in RuO_x ($x < 2$) clusters.

The stability of the adsorbed species on RuHAp-10 min was probed by heating the sample preequilibrated with CO to 250 °C in an Ar flow. The corresponding series of DRIFT spectra is shown in Fig. 2c. As mentioned previously, purging the sample at room temperature did not cause changes in the spectra of the adsorbates, but all species disappeared by heating to 250 °C. The band at 2135 cm^{-1} and the signals below 2000 cm^{-1} vanished almost completely already at 100–150 °C, indicating that these species are weakly bonded. This behavior supports the assignment of the latter features to CO adsorbed on Ru oxide-like phase (RuO_x, $x < 2$), which is different from the RuO_2 phase, because CO adsorption on bulk metal oxides is negligible at room temperature. The other bands were attenuated with increasing temperature, and their intensity dropped dramatically between 150 and 200 °C, a behavior often reported for type II (multi)carbonyls. Moreover, by increasing the temperature to 250 °C, the bands initially present at 2075 and 2006 cm^{-1} were blue-shifted to 2084 and 2016 cm^{-1}, respectively. The shift of the former band supports the presence of two components at 2081 and 2067 cm^{-1}, the one at lower energy

Table 2
Proposed assignments of the carbonyl species following CO adsorption on Ru-containing hydroxyapatite (RuHAp-10 min), compared with available literature on supported ruthenium catalysts

Entry	Material	Species	Frequency (cm^{-1})	Ref.
1	RuHAp-10 min, as-prepared and oxidized	$(RuO_x)Ru^{n+}(CO)_3$	2135 (HF_1) and 2067 (HF_2)	This work
		$Ru^{3+}(CO)_2$	2081 (HF_2) and 2006 (LF)	
		$Ru^{n+}CO$	2049	
		$(RuO_x)Ru^{n+}(CO)$	1971 and 1934 (LF)	
2	RuHAp-10 min, reduced	Ru^0–CO	2042	This work
		Ru^0_2–CO	1900–1600, broad	
		$Ru^{n+}(CO)_3$	2142 and 2081	
3	Ru/ZrO_2, oxidized	$Ru^{3+}(CO)_2$	2135 (HF_1) and 2055 (HF_2)	[41]
		$Ru^{2+}(CO)_2$	2070 (HF_2) and 2004 (LF)	
4	Ru/TiO_2, oxidized	$Ru^{n+}(CO)_3$	2142 (HF_1) and 2084 (HF_2)	[40]
		Ru^{n+}–CO	2084 (HF_2)	
		$Ru^{n+}(CO)_2$	2084 (HF_2) and 2036 (LF)	
5	RuO_x/TiO_2	$RuO_x(CO)_n$	2134–2132 (HF_1) and 2090–2080 (HF_2)	[42]
		$RuO_x(CO)$	2000–1985 (LF_1) and 1950–1935 (LF_2)	
6	Ru/SiO_2, partially oxidized	$(RuO)_2Ru^{n+}(CO)_3$	2136 (HF_1) and 2080 (HF_2)	[51]
		$(RuO)_2Ru^{n+}$–CO	2080 (HF_2)	
7	Ru/SiO_2, reduced	$(SiO)_2Ru^{n+}(CO)_3$	2144 (HF_1) and 2082 (HF_2)	[51]
8	Ru/Al_2O_3	$(RuO)_xRu^{n+}(CO)_3$	2130 (HF_1) and ~2070 (HF_2)	[44]
		$(AlO)_xRu^{n+}(CO)_3$	2140 (HF_1) and ~2080 (HF_2)	
		$Ru^{2+}(CO)_2$	~2080 (HF_2) and 2015 (LF)	
		Ru^{n+}–CO	~2080	

appearing less stable. The less stable component at 2067 cm^{-1} is likely associated with the band at 2135 cm^{-1} and thus to tricarbonyl species [$Ru^{n+}(CO)_3$], which could also be associated with the RuO_x-like phase [$(RuO_x)Ru^{n+}(CO)_3$] [44]. The persistence of the bands at 2084 and 2016 cm^{-1} with temperature indicates that they are coupled and belong to a dicarbonyl $Ru^{3+}(CO)_2$. This species is likely associated with the presence of isolated Ru^{3+} ions.

The band at 2049 cm^{-1} disappeared between 150 and 200 °C. Although it well coincides in position with the characteristic band of Ru^0 CO species [40], its behavior in Fig. 2a is not typical for dispersed metallic ruthenium because its intensity does not decrease under inert gas at room temperature, but is slightly attenuated during CO adsorption. In fact, the band for the Ru^0–CO species found during CO adsorption on reduced RuHAp-10 min at about the same position (2042 cm^{-1}) is slightly attenuated by purging with Ar at 25 °C (see later in Fig. 5). The band at 2049 cm^{-1} in the as-prepared sample might be assigned to a HF_2 band of type III (di)carbonyls [41] or to monocarbonyl species ($Ru^{n+}CO$) [20].

Concomitant with the disappearance of some signals at 150 °C, a new band developed at ca. 1862 cm^{-1}, that also blue-shifted to 1874 cm^{-1} with increasing temperature. This feature is similar to that observed on RuHAp specimen treated above 100 °C under inert atmosphere [9] and on oxidized RuHAp-10 min (Figs. 1c and 1d). Simultaneously, the HAp material was progressively dehydrated, as revealed by the increasingly negative signal at ca. 1640 cm^{-1} due to the removal of water.

Additional insight into the nature of Ru sites was obtained by oxidizing RuHAp-10 min in situ at room temperature before CO adsorption. Fig. 3 shows that the position of the bands did not change significantly on the oxidized sample compared to the as-prepared catalyst (Fig. 2a). A major difference between the two samples is the attenuation of the band at 2135 cm^{-1} and the lower ratio between the signals at 2070 (2008) cm^{-1} and 2049 cm^{-1} on the oxidized sample. This deviation suggests that the isolated Ru^{3+} ions are less perturbed by the oxygen treatment at room temperature than the Ru-oxide phase. Transformation of the species representative for the RuO_x-like phase by oxygen is best illustrated by the appearance of the negative feature at 1887 cm^{-1} with a positive counterpart at 1846 cm^{-1}. In addition, the extent of CO_2 evolution on this sample was about 50% lower than observed on the same catalyst without preoxidation (Fig. 2a), and this change appears to be related to the lower intensity of the bands at 2075 and 2006 cm^{-1} and of the low-energy side of the envelope. Apparently, the oxygen treatment before CO adsorption slows down the subsequent reductive restructuring of Ru-oxide during CO adsorption.

The nature of the band at ca. 1880 cm^{-1} appears to be an important feature of the RuHAp catalysts. We previously reported [9] a band at 1887 cm^{-1} in the DRIFT spectra of heat-treated RuHAp and RuCoHAp catalysts that is absent in HAp and in the as-prepared samples (Fig. 1). This band indicates an irreversible process involving Ru when the catalyst is heated to about 100 °C or higher. On the oxidized RuHAp-10 min, the intensity of this band decreased during CO adsorption (Fig. 1e); therefore, the band appears in the subtracted spectra during CO adsorption as a negative band (see later in Figs. 6 and 7). This band is not present in the IR spectra of RuHAp-10 min reduced in H_2 at 300 °C (Figs. 1f and 5). The increased intensity of this band for samples pretreated with O_2 at room temperature and higher temperatures in Ar, its absence in the reduced sample and its disappearance on CO adsorption on oxidized RuHAp-10 min confirm the presence of an oxidic phase that in the as-prepared sample is likely strongly hydrated. A band at 1880 cm^{-1} was previously assigned to the 2ν overtone of the

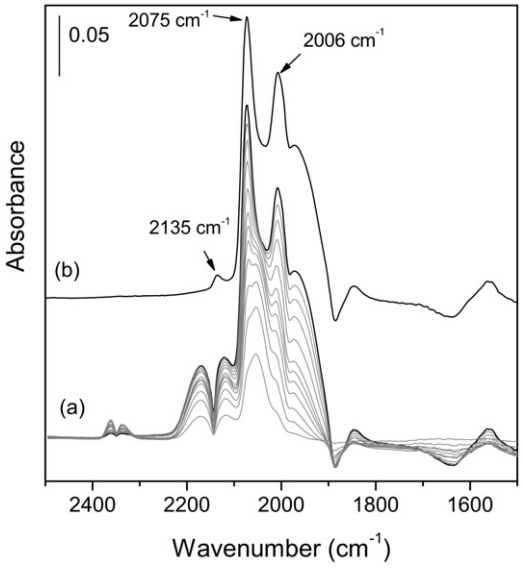

Fig. 3. (a) Time-resolved DRIFT spectra of CO adsorption on RuHAp-10 min pretreated in situ in O_2. (b) DRIFT spectrum recorded after 30 min flushing with Ar subsequent to CO adsorption. The temperature was 25 °C throughout the experiment.

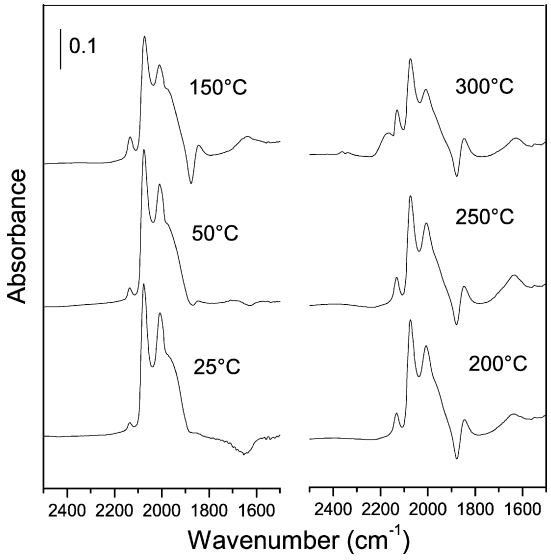

Fig. 4. DRIFT spectra of RuHAp-10 min after adsorption of CO followed by desorption in Ar. Prior to CO adsorption, the catalyst was pretreated in Ar at 25 (reference), 50, 150, 200, 250, and 300 °C.

Ru^{4+}=O mode on oxidized Ru/TiO_2 [40], and overtones have to be expected in this region for a number of oxides [45,46]. The fundamental Ru^{4+}=O vibration has been found at ca. 900 cm^{-1} on RuO_2/silica that strongly supports the appearance of an overtone at $\nu > 1800$ cm^{-1} [47]. The presence of such signal in RuHAp-10 min pretreated in O_2 at room temperature (Fig. 1c) and in Ar at 90 °C (Fig. 1d) is thus justified by the partial oxidation of Ru^{n+} ions to Ru^{4+} in a hydrated RuO_x phase. On its turn, this phase may be partially reduced on adsorption of CO (Fig. 1e), thus affording very similar species to those found on the as-prepared RuHAp-10 min catalyst (i.e., not oxidized or thermally treated). Therefore, this oxidic phase does not appear to correspond to bulk RuO_2, in agreement with the EXAFS data, indicating that the average structure of Ru in RuHAp differs from that of RuO_2 [11]. The same oxidation process occurs also when RuHAp-10 min is pretreated in Ar at 90 °C (Fig. 1d). In that case, the oxygen present on the surface of the apatite may play the role of the oxidizing agent.

In another series of experiments, RuHAp-10 min was heated from room temperature up to 300 °C in Ar before CO adsorption. The carbonyl bands on the DRIFT spectra, obtained after flushing with Ar, are shown in Fig. 4. The negative band at ca. 1880 cm^{-1}, which is characteristic of RuO_2 [9], increased with increasing pretreatment temperature. A feasible interpretation is that an increasing fraction of RuO_2 phase is formed during heat treatment and reduced afterward on CO adsorption. The intensity of the pair of bands at ca. 1970 cm^{-1} was gradually attenuated with increasing temperature and the shoulder at 1936 cm^{-1} vanished above 200 °C. These results suggest that thermal treatments induce restructuring of RuHAp-10 min. In particular, the RuO_x phase ($x < 2$) present in the as-prepared sample and characterized by the carbonyl species at 1970 and 1936 cm^{-1} converts at elevated temperature into a RuO_2-like phase indicated by the band at 1880 cm^{-1}. Note that in the same temperature range, HAp undergoes phase transition from monoclinic to hexagonal [48] and strongly dehydrates [36,37].

Because no reducing agent is applied in the preparation of RuHAp, it is not expected that metallic Ru would be present in the as-prepared catalysts. To prove this assumption, CO adsorption was studied on RuHAp-10 min after reduction of the sample in flowing H_2 at 300 °C (Fig. 5). Adsorption of CO is shown by four bands at 2142, 2081, 2042, and 1972 cm^{-1}. An important deviation is the rapid development of the bands compared with the unreduced samples. The presence of metal particles on which CO forms linear carbonyls is indicated by the band at 2042 cm^{-1} (type I carbonyls, Ru^0–CO). The broad band between 1900 to 1600 cm^{-1} can be ascribed to Ru_2–CO bridge species [49,50]. The assignment of these features to metallic Ru is supported also by the slight attenuation of the bands on replacement of CO by Ar [20].

The probable origin of the HF_1 and HF_2 bands of Ru^{n+} cations after reduction at relatively high temperature is the partial oxidation of Ru^0 by CO in a complex process involving the hydroxyl groups of the support, or disproportionation and dissociation of CO [20]. The bands at 2142 and 2081 cm^{-1} appear to follow different kinetics than those assigned to CO adsorption on metallic Ru. The slight increase in frequency of the HF_1 band (2142 cm^{-1}) on the reduced sample compared with the band developed on the as-prepared catalyst (2135 cm^{-1}) reveals the existence of two different species producing tricarbonyls on CO adsorption. Similarly, a set of three bands at 2144 (HF_1), 2082 (HF_2), and 2047 (LF) cm^{-1} was found on CO adsorption on reduced Ru/SiO_2 and the set changed into bands at 2136, 2080, and 2032 cm^{-1} on the partially oxidized sample [51]. Similarly, two different tricarbonyl species absorbed at 2140–2080 cm^{-1} and 2130–2070 cm^{-1} on Ru/Al_2O_3 [44]. Therefore, in analogy to the literature data, we tentatively assign the HF_1 and HF_2 bands observed in Fig. 5 to tricarbonyl

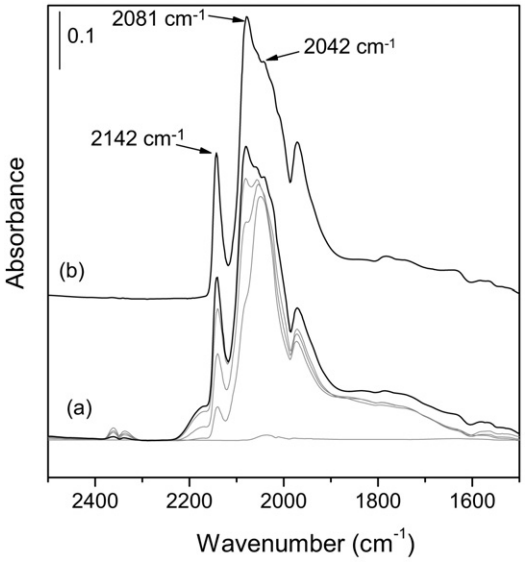

Fig. 5. (a) Time-resolved DRIFT spectra during CO adsorption at 25 °C on RuHAp-10 min pretreated in situ at 300 °C in H_2. (b) DRIFT spectrum recorded after 30 min under Ar flow after CO adsorption at 25 °C. Adsorption time (a): 1, 3, 5, 9, and 60 min.

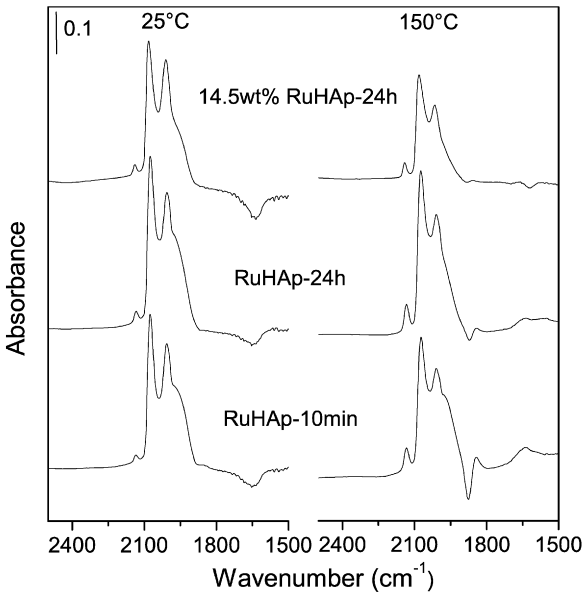

Fig. 6. DRIFT spectra of RuHAp-10 min, RuHAp-24 h, and 14.5 wt% RuHAp-24 h after adsorption of CO followed by desorption in Ar. Prior to CO adsorption the catalysts were either pretreated at 150 °C in Ar (right) or they were used without pretreatment (25 °C, left).

species adsorbed on isolated Ru^{3+} ions directly bound to the apatite support.

The left panel of Fig. 6 shows the spectra of adsorbed CO on all three untreated RuHAp catalysts. The position of the carbonyl bands is the same in the case of RuHAp-10 min and RuHAp-24 h, whereas there is a blue shift by 6 cm^{-1} in the case of 14.5 wt% RuHAp-24 h, probably because of the higher Ru content of this sample. The spectra appear very similar but differ significantly in the intensity of the low-energy shoulder below 2000 cm^{-1}, which we assigned to the presence of a RuO_x phase ($x < 2$). The intensity decreased in the sequence RuHAp-10 min > RuHAp-24 h > 14.5 wt% RuHAp-24 h. Therefore, the highest fraction of this phase seems to be present in RuHAp-10 min.

The right panel of Fig. 6 shows the spectra of adsorbed CO on the RuHAp catalysts pretreated in Ar at 150 °C. The most evident difference between the samples is the change in the intensity of the negative band at 1880 cm^{-1}, which is the most negative in case of RuHAp-10 min and becomes less negative in the same sequence as the bands below 2000 cm^{-1} decrease. This band is barely seen in the case of 14.5 wt% RuHAp-24 h. These differences indicate that the pretreatment at 150 °C induced the formation of the highest amount of the RuO_2 phase in the RuHAp-10 min catalyst. In other words, the oxidizability of the RuHAp catalysts is correlated with the amount of the RuO_x phase ($x < 2$). A careful inspection of the spectra reveals also that the bands of the dicarbonyl and monocarbonyl species on Ru^{3+} ions were enhanced from RuHAp-10 min to RuHAp-24 h, which agrees well with the previous interpretation of the fraction of the RuO_x-like phase.

The DRIFT spectra of the three RuHAp catalysts oxidized at 90 °C before CO adsorption are shown in Fig. 7. The left panel displays the spectra recorded on the neat catalyst powders, whereas the right panel shows the spectral region of the overtone of the Ru^{4+}=O fundamental in the spectra measured against KBr. As already observed in Fig. 6, the negative band at 1880 cm^{-1} is practically absent in the spectra of the 14.5 wt% RuHAp-24 h, independent of the pretreatment (Fig. 7, right panel). On the other hand, the band has the highest intensity on the oxidized RuHAp-10 min sample, corroborating that the oxidized RuHAp-10 min catalyst shows the highest amount of the RuO_2 phase, followed by the oxidized RuHAp-24 h, in agreement with the data shown in Fig. 6. This phase is partially reduced by adsorption of CO, as it is clearly indicated in the right panel of Fig. 7.

To sum up, the DRIFT study uncovered some fundamental features of the RuHAp catalysts. The presence of two major species in the as-prepared catalysts could be confirmed: isolated Ru^{3+} ions and Ru-oxide particles. The latter structure probably corresponds to a strongly hydrated Ru^{3+}-oxide; the presence of RuO_2 could be excluded, in agreement with a former EXAFS study [11]. This hydrated oxide can be (partially) oxidized by pure oxygen to hydrated Ru^{4+}-oxide (RuO_2) already at room temperature, and reduced by CO to a lower valence state carbonyl species or by hydrogen (at 300 °C) to metallic Ru (Ru^0). In contrast, the isolated Ru^{3+} ions are less reactive in oxidation by oxygen at 25–90 °C, indicating their lower reactivity in redox reactions. (In this respect, the DRIFT study is not conclusive: Isolated Ru^{3+} ions may either be less reactive than hydrated Ru^{3+}-oxide or not reactive at all.) It is also shown that the oxidizability of the investigated RuHAp catalysts correlates well with the amount of hydrated Ru^{3+}-oxide phase (RuHAp-10 min > RuHAp-24 h > 14.5 wt% RuHAp-24 h).

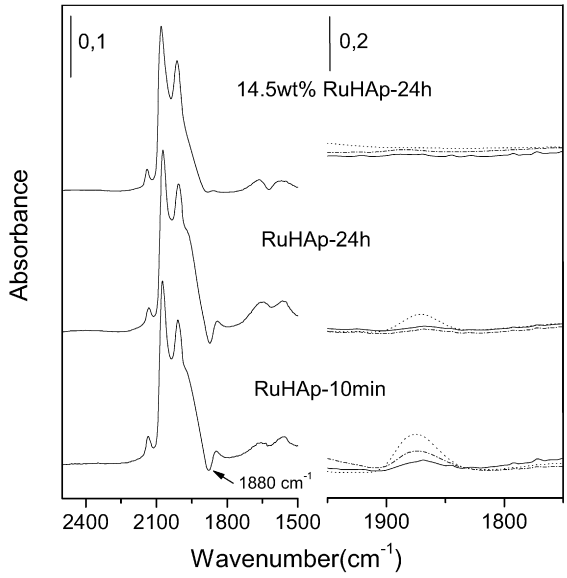

Fig. 7. (Left panel) DRIFT spectra of RuHAp-10 min, RuHAp-24 h, and 14.5 wt% RuHAp-24 h after adsorption of CO followed by desorption in Ar. The catalysts were pretreated in O_2 at 90 °C prior to CO adsorption. (Right panel) DRIFT spectra of the same specimen before pretreating with O_2 (solid), after pretreating with O_2 (dot) and after CO adsorption (dash dot).

3.2. Reducibility of RuHAp

According to the probable reaction mechanism of alcohol oxidation with oxygen on RuHAp, the Ru-alcoholate intermediate undergoes β-hydride elimination to afford the carbonyl compound and Ru-hydride [10]. The hydrido-Ru species is inactive in alcohol oxidation [11] and needs to be reoxidized by oxygen to complete the redox cycle. The presence of reduced Ru sites in the working catalyst was proven by EXAFS analysis [11]. An important conclusion from this mechanism is that the active Ru species should be easily reducible to achieve reasonable reaction rates. It is known from earlier studies [9,10] that the order of activity of Ru-hydroxyapatites in the aerobic oxidation of alcohols is the following: RuHAp-10 min > RuHAp-24 h > 14.5 wt% RuHAp-24 h. Because bulky substrates may not reach some Ru sites located in the narrow channels of HAp, we applied hydrogen, the smallest possible reducing agent, to characterize the reducibility, and thus indirectly the alcohol dehydrogenation activity, of Ru-hydroxyapatites.

The reducibility of the catalysts was determined at 40 °C. The difference between the hydrogen consumption in the first and second runs yields the amount of H_2 consumption (H), according to the double-isotherm method [32]. The amount of hydrogen consumption related to the amount of ruthenium (H/Ru) in the catalysts is used to compare the reducibility of the Ru sites in the catalysts. Table 3 shows that RuHAp-10 min contains the highest specific amount of reducible Ru, followed by RuHAp-24 h and the 14.5 wt% RuHAp-24 h. This order is the same as the reactivity order derived from alcohol oxidation reactions and indicates that the contribution of poorly accessible Ru sites in the HAp matrix does not distort the correlation. In addition, the specific reducibility of the catalysts by hydrogen correlates well with the amount of Ru^{3+}-oxide phase derived from CO adsorption by DRIFT.

Table 3
Hydrogen consumption (H) in the reduction of RuHAp catalysts at 40 °C

Sample	H/Ru (at%)
2.6 wt% RuHAp-10 min	100
3.2 wt% RuHAp-24 h	69
14.5 wt% RuHAp-24 h	38

3.3. TEM analysis

HAADF-STEM images of the RuHAp samples reveal that the apatite crystals are more or less homogeneously covered by bright spots of 1–2 nm in diameter (Fig. 8). The bright spots represent the sites where Ru is located because Ru is the strongest scatterer in this system (highest atomic number). The presence of Ru in the apatite matrix was confirmed by EDX analysis (not shown). Interestingly, no significant difference could be observed between the images of the different RuHAp samples; the size and distribution of the Ru clusters appear very similar on all three catalysts. On the basis of the DRIFT analysis, it is very probable that the bright spots correspond to hydrated Ru-oxide nanoparticles, dispersed on the apatite surface.

The possibility that the observed features appear as a consequence of the reduction of Ru^{3+} to metallic Ru by the electron beam can be discarded. In fact, there is no significant change between the HAADF-STEM image of RuHAp-10 min before and after reduction in flowing hydrogen at 300 °C (Figs. 8a and 8d). In contrast, after pretreatment of the same catalyst in oxygen at 90 °C the Ru-containing nanoparticles are redispersed and the bright spots are barely distinguishable (Fig. 8e). In the light of the DRIFT results, this change is probably correlated with the (partial) formation of Ru^{4+}-oxide.

3.4. Catalyst structure: Nature of active redox sites

To identify the Ru-containing species in the Ru-exchanged HAp catalysts, we used DRIFT spectroscopy of CO adsorption, electron microscopy, and hydrogen reduction under close to ambient conditions. Although the infrared spectra were rather complex due to changes in the oxidation state of Ru induced by CO adsorption at room temperature and the concomitant evolution of CO_2, interpretation of the spectra is supported by the abundant information available in the literature on various supported Ru-containing catalysts [20,40–42,44,51]. Our study confirmed the presence of isolated, monomeric Ru^{3+} cations in all three RuHAp catalysts investigated here (Table 1). The isolated Ru^{3+} cations produce carbonyl species on CO adsorption that are stable against desorption up to ca. 200 °C. Until now, these species have been considered the active sites in the aerobic oxidation of alcohols in the liquid phase, at around 40–110 °C [9–13,17]. Besides monomeric Ru^{3+} cations, we could identify a hydrated Ru^{n+}-oxide phase by DRIFT study

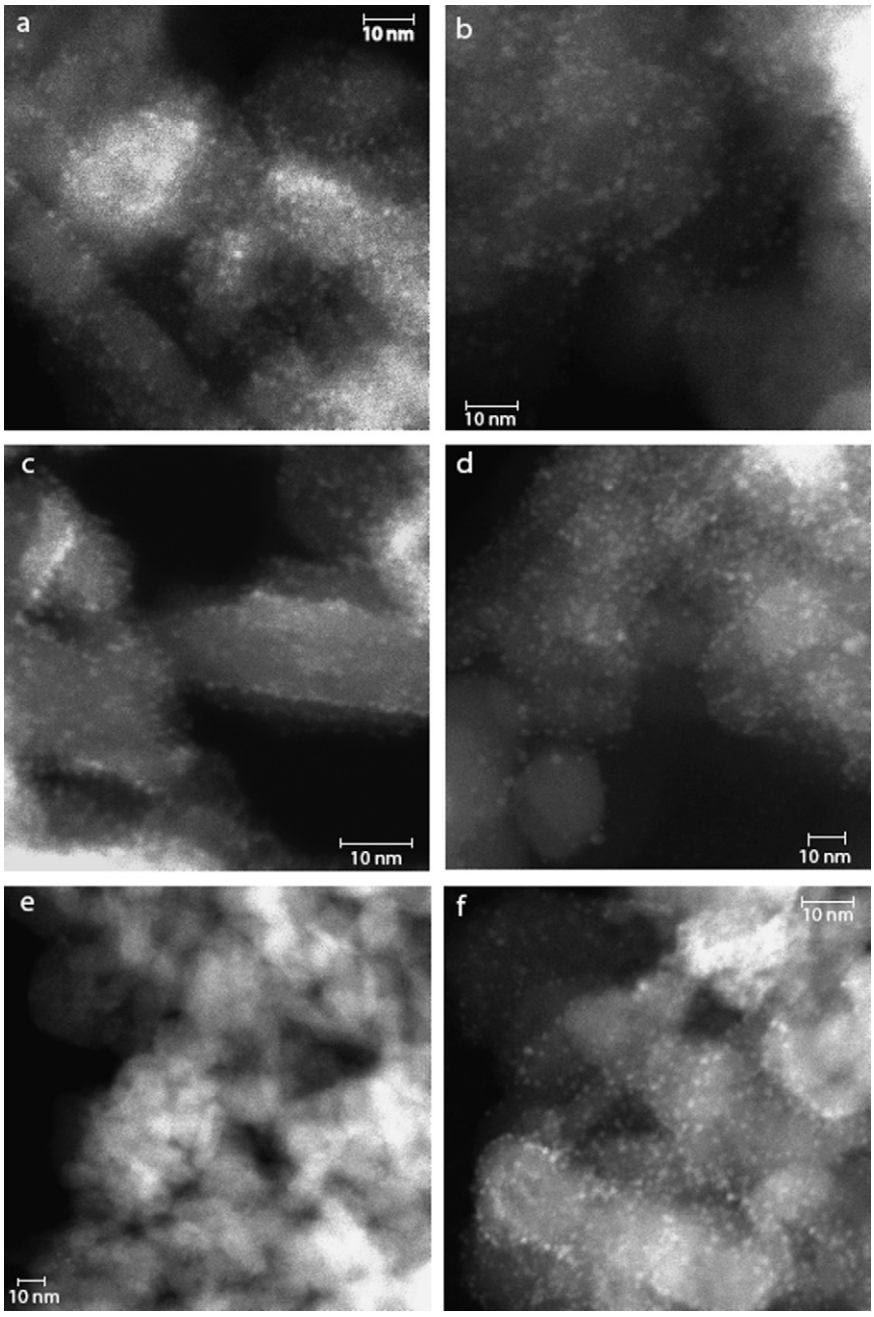

Fig. 8. HAADF-STEM images of (a) RuHAp-10 min, (b) RuHAp-24 h, (c) 14.5 wt% RuHAp-24 h, (d) RuHAp-10 min pretreated with H_2 at 300 °C, (e) RuHAp-10 min pretreated with O_2 at 90 °C, and (f) RuHAp-10 min after benzyl alcohol oxidation. The HAp crystals are covered by Ru particles (bright spots).

in all catalysts. The oxidation state of the Ru in the Ru^{n+}-oxide phase should be 3+, because the Ru^{+} and Ru^{2+} oxides are unstable, and the presence of Ru^{4+} in the as-prepared material could be excluded. In addition, the oxidation state of Ru^{3+} in RuHAp was confirmed by EPR analysis [17]. The complementary HAADF-STEM study provided a strong support to this discovery by visualizing the nanosized Ru^{3+}-oxide particles. This phase produced the asymmetric broadening below 2000 cm^{-1} and the tricarbonyl species at 2135 and 2081 cm^{-1}. RuO_2 could not be detected in any of the untreated ("as-prepared") catalysts.

In contrast to the monomeric Ru^{3+} cations, the hydrated Ru^{3+}-oxide phase was highly active in redox reactions. It was converted to RuO_2 already at room temperature with pure oxygen (Fig. 1c) and partially reduced by CO (Figs. 3, 4, 6, and 7). Under more severe conditions, at 300 °C, also metallic Ru was formed with hydrogen. The considerable hydrogen consumption already at 40 °C (H/Ru = 0.38–1.0, Table 3) is also attributed to this phase, because the amount of the hydrated Ru^{3+}-oxide phase correlates well with the amount of hydrogen consumed by these catalysts (RuHAp-10 min > RuHAp-24 h > 14.5 wt% RuHAp-24 h). The amount of hydrated RuO_2

phase, produced by pretreatment with oxygen, and the catalytic activity in alcohol oxidation with molecular oxygen follow the same order. All these observations suggest that the real active species in RuHAp are hydrated Ru^{3+}-oxide nanoparticles located at the surface of HAp.

The amount of hydrated Ru^{3+}-oxide depends on the contact time between HAp and the aqueous $RuCl_3$ solution, as well as on the $RuCl_3$ concentration. The infrared data indicate that its fraction decreased with long contact time and high Ru concentration. To understand this point, we analyzed the mechanism of incorporation of Ru^{3+} ions from aqueous solutions into HAp. We have shown that on contacting HAp with the aqueous $RuCl_3$ solution, the acidity of the solution decreased and more than a stoichiometric amount of Ca^{2+} and significant amount of PO_4^{3-} ions dissolved [9]. Clearly, this process cannot be described simply as an ion exchange between Ca^{2+} and Ru^{3+} ions. We assume that the first step in the genesis of RuHAp is the adsorption of Ru^{3+} ions on the basic sites of HAp, followed by the formation of Ru-hydroxide (hydrated Ru^{3+}-oxide). Dissolution of HAp accompanied by the precipitation of a new Ru-containing phosphate phase is also a feasible process [28]. Dissolution is favored by the higher acidity of the more concentrated $RuCl_3$ solution and the longer contact time. The considerable restructuring and partial loss of the crystalline apatite phase during the 24 h contact time period has been demonstrated by XRD analysis [9].

Extensive exchange of the Ca^{2+} ions in HAp necessitates the solid-state diffusion of Ru^{3+} ions into HAp, but the channels are very narrow (<0.3 nm) and occupied by the OH^- ions [52]. This process is expected to be slow, and the Ru sites located in the narrow channels are not accessible for bulky organic substrates. Because no significant negative effect of the steric bulkiness of the alcohol substrate has been observed [9], the contribution of Ru^{3+} in the HAp channels can be excluded. Replacement of some Ca^{2+} ions at the outer surface of HAp and subsequent production of monomeric Ru^{3+} sites seem to be more relevant for catalysis. But this process should be fast, and it cannot explain the changes occurring during extended contact time. The processes occurring during long contact times (24 h) produce less accessible and/or catalytically less active Ru species, as indicated by the lower TOF values in alcohol oxidation. This interpretation is supported by the hydrogen consumption measurements (Table 3) demonstrating the greatest reduction of the RuHAp catalyst with short contact time. As mentioned previously, reducibility of the active species is crucial, as hydrido-Ru species are formed during alcohol oxidation.

Finally, there is ample evidence that Ru^{3+}-hydroxide (or hydrated oxide) [53,54] and hydrated RuO_2 [29,30,55,56] are active and selective in the aerobic oxidation of alcohols. In contrast, it has been speculated that monomeric Ru^{3+} ions in HAp are active, but to date, no evidence of this has been provided.

Characterization of the active Ru species in RuHAp may be refined by analyzing in more detail the changes in the high-frequency region (>3000 cm^{-1}) on adsorption of probe molecules, and by extending the experimental conditions including vacuum and low temperature, and to adsorption from the liquid phase. Measurements in these directions are presently performed in our laboratory.

4. Conclusion

We have revisited the nature of Ru sites in RuHAp that are responsible for the activity and selectivity of these catalysts in the aerobic oxidation of alcohols to aldehydes and ketones using DRIFT spectroscopy combined with CO adsorption. To gain insight into the nature of the complex infrared spectra, we studied the catalysts in the as-prepared state and after exposure to oxygen and hydrogen, as well as at increasing temperature in Ar before CO adsorption. A set of six bands was observed on as-prepared RuHAp in the 2150–1950 cm^{-1} spectral range. The desorption behavior of the species giving rise to these bands and their different ratios in the oxidized sample and in that treated at increasing temperature in inert gas before CO adsorption reveal that the bands can be attributed to two species: (i) monomeric Ru^{3+} ions, likely located at the apatite surface, and (ii) labile $Ru_2O_3 \cdot xH_2O$, which is far more active in reduction and oxidation reactions than the isolated Ru^{3+} ions. The presence of 1–2 nm Ru-containing nanoparticles was evidenced by STEM-EDX. All observations in this study and data from the pertinent literature are in agreement with our proposal that the highly dispersed, hydrated Ru-oxide particles are the true active sites in the aerobic oxidation of alcohols. Future studies need to clarify whether this conclusion is also valid for other reactions, such as the oxidation of amines and organosilanes, that are catalyzed by RuHAp.

Acknowledgments

Financial support for this work was provided by ETH Zurich. We thank the Electron Microscopy ETH Zurich, EMEZ, for support.

References

[1] S. Sugiyama, T. Shono, D. Makino, T. Moriga, H. Hayashi, J. Catal. 214 (2003) 8.
[2] K. Elkabouss, M. Kacimi, M. Ziyad, S. Ammar, F. Bozon-Verduraz, J. Catal. 226 (2004) 16.
[3] B.M. Choudary, C. Sridhar, M.L. Kantam, B. Sreedhar, Tetrahedron Lett. 45 (2004) 7319.
[4] Y. Maeda, Y. Washitake, T. Nishimura, K. Iwai, T. Yamauchi, S. Uemura, Tetrahedron 60 (2004) 9031.
[5] Z. Boukha, M. Kacimi, M.F.R. Pereira, J.L. Faria, J.L. Figueiredo, M. Ziyad, Appl. Catal. A 317 (2007) 299.
[6] S. Sugiyama, S. Tanimoto, K. Fukuda, K. Kawashiro, T. Tomida, H. Hayashi, Colloids Surf. A 252 (2005) 187.
[7] M. Wakamura, K. Kandori, T. Ishikawa, Colloids Surf. A 142 (1998) 107.
[8] M. Wakamura, K. Kandori, T. Ishikawa, Colloids Surf. A 164 (2000) 297.
[9] Z. Opre, J.D. Grunwaldt, M. Maciejewski, D. Ferri, T. Mallat, A. Baiker, J. Catal. 230 (2005) 406.
[10] K. Yamaguchi, K. Mori, T. Mizugaki, K. Ebitani, K. Kaneda, J. Am. Chem. Soc. 122 (2000) 7144.
[11] Z. Opre, J.D. Grunwaldt, T. Mallat, A. Baiker, J. Mol. Catal. A Chem. 242 (2005) 224.
[12] Z. Opre, D. Ferri, F. Krumeich, T. Mallat, A. Baiker, J. Catal. 241 (2006) 287.

[13] K. Tonsuaadu, M. Gruselle, F. Villain, R. Thouvenot, M. Peld, V. Mikli, R. Traksmaa, P. Gredin, X. Carrier, L. Salles, J. Colloid Interface Sci. 304 (2006) 283.
[14] K. Mori, K. Yamaguchi, T. Mizugaki, K. Ebitani, K. Kaneda, Chem. Commun. (2001) 461.
[15] K. Mori, M. Tano, T. Mizugaki, K. Ebitani, K. Kaneda, New J. Chem. 26 (2002) 1536.
[16] K. Mori, T. Hara, T. Mizugaki, K. Ebitani, K. Kaneda, J. Am. Chem. Soc. 125 (2003) 11460.
[17] S. Wuyts, D.E. De Vos, F. Verpoort, D. Depla, R. De Gryse, P.A. Jacobs, J. Catal. 219 (2003) 417.
[18] K. Mori, S. Kanai, T. Hara, T. Mizugaki, K. Ebitani, K. Jitsukawa, K. Kaneda, Chem. Mater. 19 (2007) 1249.
[19] D. Zahn, O. Hochrein, Phys. Chem. Chem. Phys. 5 (2003) 4004.
[20] K.I. Hadjiivanov, G.N. Vayssilov, Adv. Catal. 47 (2002) 307.
[21] T. Suzuki, T. Hatsushika, Y. Hayakawa, J. Chem. Soc. Faraday Trans. I 77 (1981) 1059.
[22] T. Suzuki, T. Hatsushika, M. Miyake, J. Chem. Soc. Faraday Trans. I 78 (1982) 3605.
[23] Y. Takeuchi, H. Arai, J. Chem. Eng. Jpn. 23 (1990) 75.
[24] J. Jeanjean, U. Vincent, M. Fedoroff, J. Solid State Chem. 108 (1994) 68.
[25] J.J. Middelburg, R.N.J. Comans, Chem. Geol. 90 (1991) 45.
[26] Q.Y. Ma, S.J. Traina, T.J. Logan, J.A. Ryan, Environ. Sci. Technol. 27 (1993) 1803.
[27] Y.P. Xu, F.W. Schwartz, S.J. Traina, Environ. Sci. Technol 28 (1994) 1472.
[28] E. Valsami-Jones, K.V. Ragnarsdottir, A. Putnis, D. Bosbach, A.J. Kemp, G. Cressey, Chem. Geol. 151 (1998) 215.
[29] M. Musawir, P.N. Davey, G. Kelly, I.V. Kozhevnikov, Chem. Commun. (2003) 1414.
[30] B.Z. Zhan, M.A. White, T.K. Sham, J.A. Pincock, R.J. Doucet, K.V.R. Rao, K.N. Robertson, T.S. Cameron, J. Am. Chem. Soc. 125 (2003) 2195.
[31] S. Sugiyama, T. Minami, H. Hayashi, M. Tanaka, N. Shigemoto, J.B. Moffat, J. Chem. Soc. Faraday Trans. 92 (1996) 293.
[32] J.H. Sinfelt, D.J.C. Yates, J.L. Carter, J. Catal. 24 (1972) 283.
[33] S.J. Pennycook, Ultramicroscopy 30 (1989) 58.
[34] J. Liu, Microsc. Microanal. 10 (2004) 55.
[35] S. Koutsopoulos, J. Biomed. Mater. Res. 62 (2002) 600.
[36] M.I. Zaki, H. Knözinger, B. Tesche, Langmuir 22 (2006) 749.
[37] L. Bertinetti, A. Tampieri, E. Landi, C. Ducati, P.A. Midgley, S. Coluccia, G. Martra, J. Phys. Chem. B 111 (2007) 4027.
[38] H. Tanaka, M. Chikazawa, K. Kandori, T. Ishikawa, Phys. Chem. Chem. Phys. 2 (2000) 2647.
[39] T. Ishikawa, M. Wakamura, S. Kondo, Langmuir 5 (1989) 140.
[40] K. Hadjiivanov, J.C. Lavalley, J. Lamotte, F. Mauge, J. Saint-Just, M. Che, J. Catal. 176 (1998) 415.
[41] E. Guglielminotti, F. Boccuzzi, M. Manzoli, F. Pinna, M. Scarpa, J. Catal. 192 (2000) 149.
[42] N.M. Gupta, V.S. Kamble, R.M. Iyer, K.R. Thampi, M. Grätzel, J. Catal. 137 (1992) 473.
[43] T. Mizushima, K. Tohji, Y. Udagawa, A. Ueno, J. Phys. Chem. 94 (1990) 4980.
[44] S.Y. Chin, C.T. Williams, M.D. Amiridis, J. Phys. Chem. B 110 (2006) 871.
[45] G. Busca, J.C. Lavalley, Spectrochim. Acta Part A 42 (1986) 443.
[46] A.A. Davydov, in: N.T. Sheppard (Ed.), Molecular Spectroscopy of Oxide Catalyst Surfaces, Wiley, Chichester, 2003.
[47] T. Lopez, P. Bosch, M. Asomoza, R. Gomez, J. Catal. 133 (1992) 247.
[48] I. Reisner, W.E. Klee, Spectrochim. Acta Part A 38 (1982) 899.
[49] C.S. Kellner, A.T. Bell, J. Catal. 71 (1981) 296.
[50] C. Elmasides, D.I. Kondarides, W. Grunert, X.E. Verykios, J. Phys. Chem. B 103 (1999) 5227.
[51] G.H. Yokomizo, C. Louis, A.T. Bell, J. Catal. 120 (1989) 1.
[52] C. Rey, in: P.W. Brown, B. Constantz (Eds.), Hydroxyapatite and Related Materials, CRC Press, 1994, p. 257.
[53] D.V. Bavykin, A.A. Lapkin, P.K. Plucinski, J.M. Friedrich, F.C. Walsh, J. Catal. 235 (2005) 10.
[54] K. Yamaguchi, N. Mizuno, Angew. Chem. Int. Ed. 41 (2002) 4538.
[55] M. Matsumoto, N. Watanabe, J. Org. Chem. 49 (1984) 3435.
[56] T.L. Stuchinskaya, M. Musawir, E.F. Kozhevnikova, I.V. Kozhevnikov, J. Catal. 231 (2005) 41.